Article

Phosphodiester Cleavage in Ribonuclease H Occurs via an Associative Two-Metal-Aided Catalytic Mechanism

Marco De Vivo, Matteo Dal Peraro, and Michael L. Klein

J. Am. Chem. Soc., **2008**, 130 (33), 10955-10962 • DOI: 10.1021/ja8005786 • Publication Date (Web): 29 July 2008

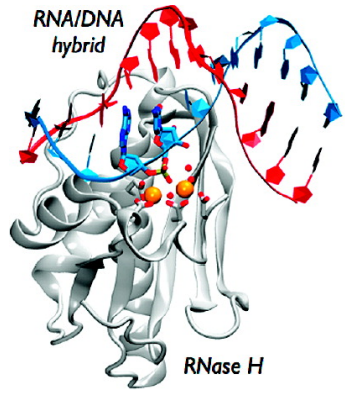

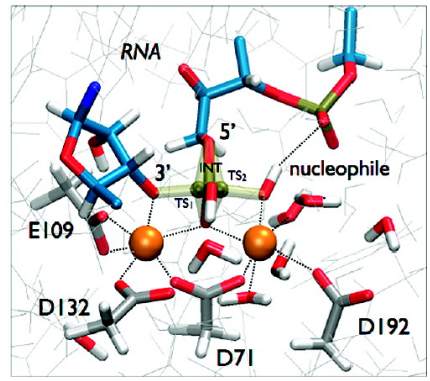

More About This Article

Additional resources and features associated with this article are available within the HTML version:

- Supporting Information
- Links to the 2 articles that cite this article, as of the time of this article download
- Access to high resolution figures
- Links to articles and content related to this article
- Copyright permission to reproduce figures and/or text from this article

View the Full Text HTML

J|A|C|S
ARTICLES

Published on Web 07/29/2008

Phosphodiester Cleavage in Ribonuclease H Occurs via an Associative Two-Metal-Aided Catalytic Mechanism

Marco De Vivo,*,†,‡ Matteo Dal Peraro,*,§ and Michael L. Klein†

Center for Molecular Modeling and Department of Chemistry, University of Pennsylvania, 231 South 34th Street, Philadelphia, Pennsylvania 19104-6323, and Laboratory for Biomolecular Modeling, Institute of Bioengineering, School of Life Sciences, Ecole Polytechnique Fédérale de Lausanne, EPFL, CH-1015 Lausanne, Switzerland

Received January 30, 2008; E-mail: mdevivo@cmm.upenn.edu; matteo.dalperaro@epfl.ch

Abstract: Ribonuclease H (RNase H) belongs to the nucleotidyl-transferase (NT) superfamily and hydrolyzes the phosphodiester linkages that form the backbone of the RNA strand in RNA•DNA hybrids. This enzyme is implicated in replication initiation and DNA topology restoration and represents a very promising target for anti-HIV drug design. Structural information has been provided by high-resolution crystal structures of the complex RNase H/RNA•DNA from *Bacillus halodurans* (Bh), which reveals that two metal ions are required for formation of a catalytic active complex. Here, we use classical force field-based and quantum mechanics/molecular mechanics calculations for modeling the nucleotidyl transfer reaction in RNase H, clarifying the role of the metal ions and the nature of the nucleophile (water versus hydroxide ion). During the catalysis, the two metal ions act cooperatively, facilitating nucleophile formation and stabilizing both transition state and leaving group. Importantly, the two Mg^{2+} metals also support the formation of a metastable phosphorane intermediate along the reaction, which resembles the phosphorane intermediate structure obtained only in the debated β-phosphoglucomutase crystal (Lahiri, S. D.; et al. *Science* **2003**, *299* (5615), 2067−2071). The nucleophile formation (i.e., water deprotonation) can be achieved *in situ*, after migration of one proton from the water to the scissile phosphate in the transition state. This proton transfer is actually mediated by solvation water molecules. Due to the highly conserved nature of the enzymatic bimetal motif, these results might also be relevant for structurally similar enzymes belonging to the NT superfamily.

Introduction

The nucleotidyl-transferase (NT) superfamily comprises enzymes able to catalyze the hydrolysis of phosphodiester linkages that form the backbone of DNA and RNA strands. An important class of sequence-nonspecific metallo-endonucleases, which belongs to the NT superfamily, is ribonuclease H (RNase H). In the presence of Mg^{2+} ions, the cofactors necessary for optimal activity, RNase H hydrolyzes the P−O3′ bond of the RNA strand, degrading RNA•DNA hybrids.[1] These ubiquitous enzymes are mainly implicated in replication initiation and DNA topology restore,[2,3] and due to RNase H activity in HIV reverse transcriptase (HIV-RT), it represents a promising target for anti-HIV drug design.[4,5]

High-resolution crystals have revealed the structural arrangement of the complex formed by RNase H and its substrate, the RNA•DNA hybrid.[6–9] A divalent bimetal architecture of the catalytic site has been defined, as originally proposed by Steitz and Steitz.[10] The two Mg^{2+} ions are jointly coordinated to a nonbridging oxygen of the scissile phosphate of the substrate RNA strand and are surrounded by four conserved carboxylates (D71, E109, D132 and D192, Figure 1) and water molecules. This bimetal motif of the catalytic site has been suggested for other classes of structurally similar enzymes that incorporate the highly conserved DDE motif in their sequence[11] and belong to the NT superfamily (e.g., Holliday junction resolvase, retroviral integrase, transposase, and RISC nuclease Argonaute).[12–14]

† University of Pennsylvania.
‡ Current address: Rib-X Pharmaceuticals, Inc., 300 George Street, New Haven, CT.
§ Ecole Polytechnique Federale de Lausanne.

(1) Yang, W.; Lee, J. Y.; Nowotny, M. *Mol. Cell* **2006**, *22* (1), 5–13.
(2) Broccoli, S.; Rallu, F.; Sanscartier, P.; Cerritelli, S. M.; Crouch, R. J.; Drolet, M. *Mol. Microbiol.* **2004**, *52* (6), 1769–1779.
(3) Kogoma, T.; Foster, P. L. *Ribonucleases H*; Crouch R. J., Toulme, J. J., Eds.; INSERM: Paris, 1998; pp 39−66.
(4) Klumpp, K.; Hang, J. Q.; Rajendran, S.; Yang, Y.; Derosier, A.; Wong Kai In, P.; Overton, H.; Parkes, K. E.; Cammack, N.; Martin, J. A. *Nucleic Acids Res.* **2003**, *31* (23), 6852–6859.
(5) Shaw-Reid, C. A.; Feuston, B.; Munshi, V.; Getty, K.; Krueger, J.; Hazuda, D. J.; Parniak, M. A.; Miller, M. D.; Lewis, D. *Biochemistry* **2005**, *44* (5), 1595–1606.
(6) Nowotny, M.; Gaidamakov, S. A.; Crouch, R. J.; Yang, W. *Cell* **2005**, *121* (7), 1005–1016.
(7) Nowotny, M.; Gaidamakov, S. A.; Ghirlando, R.; Cerritelli, S. M.; Crouch, R. J.; Yang, W. *Mol. Cell* **2007**, *28* (2), 264–276.
(8) Nowotny, M.; Yang, W. *EMBO J.* **2006**, *25* (9), 1924–1933.
(9) Nowotny, M.; Cerritelli, S. M.; Ghirlando, R.; Gaidamakov, S. A.; Crouch, R. J.; Yang, W. *EMBO J.* **2008**, *27* (7), 1172–1181.
(10) Steitz, T. A.; Steitz, J. A. *Proc. Natl. Acad. Sci. U.S.A.* **1993**, *90* (14), 6498–6502.
(11) Haren, L.; Ton-Hoang, B.; Chandler, M. *Annu. Rev. Microbiol.* **1999**, *53*, 245–281.
(12) Yang, W.; Steitz, T. A. *Structure* **1995**, *3* (2), 131–134.
(13) Rice, P. A.; Baker, T. A. *Nat. Struct. Biol.* **2001**, *8* (4), 302–307.
(14) Song, J. J.; Smith, S. K.; Hannon, G. J.; Joshua-Tor, L. *Science* **2004**, *305* (5689), 1434–1437.

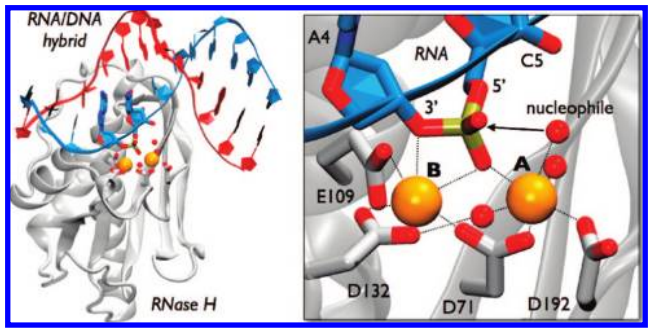

Figure 1. RNase H structural and catalytic features. (Left) Cartoon of the complex RNase H/RNA•DNA hybrid. RNase H is in gray, DNA is in red, and RNA is in blue; orange spheres indicate the Mg^{2+} ions. (Right) Close-up of the catalytic site, including the RNA strand, and key residues and water molecules coordinated to the two Mg^{2+} ions.

Stereochemical studies of RNase H activity have suggested a general reaction scheme that shows an in-line S_N2-like nucleophilic attack on the scissile phosphorus atom by the nucleophilic group that is believed to be, in its final form, one hydroxide ion.[15,16] Then, after the nucleophilic attack, the inversion of the phosphate stereo configuration and formation of the 5′-phosphate and 3′-hydroxy function of the RNA strand conclude the catalytic action (Scheme 1). Thus, the divalent metal ions have been suggested to stabilize the overall negative charge along the reaction pathway and to facilitate the formation of the nucleophilic hydroxide ion by dissociation of a metal-bound water. A hydroxide ion is the common choice as nucleophilic group when studying this type of hydrolytic mechanism.[17] In this way, the catalytic site includes a better nucleophile (i.e., the nucleophilicity of the hydroxide ion is higher than water), and the problem of water dissociation and formation of a nucleophilic hydroxide ion is overcome. However, the common assumption that one hydroxide ion is already present in the starting system explains neither the mechanism of its formation, nor the energy necessary to have such early water dissociation. In this regard, it is important to mention that the pro-R_p oxygen of the phosphate immediately 3′ to the scissile bond has been demonstrated to be essential for optimal catalysis. Experiments show that replacement of the pro-R_p oxygen with a sulfur atom reduces the k_{cat} of *Escherichia coli* RNase HI by 86%. That is, phosphorothioate substitution of the phosphate 3′ to the scissile phosphodiester bond of the substrate, in *E. coli* RNase HI, reduced the k_{cat} value of the wild-type RNase HI by 6.9-fold.[18] Indeed, this indicates a key role of the pro-R_p oxygen, suggesting either its possible role as a general base for water deprotonation (i.e., nucleophile formation) or its function to stabilize and orient the attacking hydroxide ion, through the formation of a hydrogen bond. The unclear, but critical, role of the pro-R_p oxygen is also pointed out by a stereochemical study[15] (matrix-assisted desorption/ionization time-of-flight mass spectrometry experiments) performed on *E. coli* RNase H.

Despite the proposed reaction scheme, mechanistic and dynamical details are needed to understand the bimetal-aided nucleotidyl transfer reaction. In fact, the fleeting nature of the reaction transition state allows neither a direct experimental observation of its geometrical characteristic nor one of its chemical features, leaving open important questions. Is the enzymatic mechanism concerted one-step or stepwise with formation of a stable phosphorane intermediate? How is the nucleophilic hydroxide ion formed? What is the role of the pro-R_p oxygen during the catalysis? How are the two metal cofactors aiding the catalysis?

In the effort to capture the thermodynamic aspects of catalysis, and progress to answer the aforementioned questions, we use a computational approach, which includes classical force field-based and first principles quantum mechanics/molecular mechanics calculations[19] for the modeling of the nucleotidyl transfer reaction in *Bacillus halodurans* (*Bh*) RNase H complexed with the hybrid RNA•DNA substrate.[6] We have considered two different reagent states for the enzymatic reaction: (i) first, a conformation in which the nucleophilic species is a water molecule (WAT_N), and (ii) second, one in which a hydroxide is the reactive agent (OH_N). Our computations provide a consistent interpretation of available experiments and propose an elegant enzymatic strategy for bimetal-aided nucleotidyl transfer catalysis.

Computational Materials and Methods

Structural Models. Calculations are based on the crystallographic structure of *Bacillus halodurans* RNase H complexed with the hybrid RNA•DNA substrate as in the D192N mutated conformation (pdb code 1ZBL, 2.2 Å resolution).[6] Although the mutant enzyme is completely inactive, D192N substitution supposedly does not significantly affect the active site architecture.[6] Furthermore, D192N mutation affects the active site much less than D132N mutation, which perturbs the coordination shell of the A-site Mg^{2+}.[6] For this reason, in the molecular model employed herein, N192 is replaced by D192 to reproduce the wild-type conformation. The remaining structural details of the molecular model are retained as in the crystallographic structure. This includes the Mg^{2+} ions coordination sphere in the active configuration of the enzyme upon DNA•RNA substrate binding (Figure 1).

MD Simulations. Molecular dynamics is used to equilibrate the complex at physiological conditions and provide a suitable model of the Michaelis complex for subsequent Car−Parrinello (CP) quantum mechanical/molecular mechanics (QM/MM) calculations.[20] The AMBER force field is adopted for the simulations,[21] whereas the NAMD package[22] is used as the MD engine. The metal active site is treated with a flexible nonbonded approach based on the "atoms in molecules" partitioning scheme[23] of the DFT-BLYP electronic density of the active site, as explained in detail in ref 24. This allows one to account for the charge transfer interactions between Mg^{2+} ions and their ligands and permits possible structural rearrangements at the active site during the MD simulations. More details on the MD setup procedure and rmsd data are reported in Supporting Information and ref 24. A ~25 ns classical MD trajectory is performed using a water molecule as nucleophile. The system was equilibratated within the initial ~2 ns and maintained

(15) Krakowiak, A.; Owczarek, A.; Koziolkiewicz, M.; Stec, W. J. *Chembiochem* **2002**, *3* (12), 1242–1250.
(16) Cassano, A. G.; Anderson, V. E.; Harris, M. E. *Biopolymers* **2004**, *73* (1), 110–129.
(17) Ivanov, I.; Tainer, J. A.; McCammon, J. A. *Proc. Natl. Acad. Sci. U.S.A.* **2007**, *104* (5), 1465–1470.
(18) Haruki, M.; Tsunaka, Y.; Morikawa, M.; Iwai, S.; Kanaya, S. *Biochemistry* **2000**, *39* (45), 13939–13944.
(19) Warshel, A.; Levitt, M. *J. Mol. Biol.* **1976**, *103* (2), 227–249.
(20) Laio, A.; VandeVondele, J.; Rothlisberger, U. *J. Chem. Phys.* **2002**, *116* (16), 6941–6947.
(21) Cornell, W. D.; Cieplak, P.; Bayly, C. I.; Gould, I. R.; Merz, K. M.; Ferguson, D. M.; Spellmeyer, D. C.; Fox, T.; Caldwell, J. W.; Kollman, P. A. *J. Am. Chem. Soc.* **1995**, *117* (19), 5179–5197.
(22) Kale, L.; Skeel, R.; Bhandarkar, M.; Brunner, R.; Gursoy, A.; Krawetz, N.; Phillips, J.; Shinozaki, A.; Varadarajan, K.; Schulten, K. *J. Comp. Phys.* **1999**, *151* (1), 283–312.
(23) Bader R. F. W. *Atoms in Molecule: A Quantum Theory*; Oxford University Press: Oxford, 1990.
(24) Dal Peraro, M.; Spiegel, K.; Lamoureux, G.; De Vivo, M.; DeGrado, W. F.; Klein, M. L. *J. Struct. Biol.* **2007**, *157* (3), 444–453.

Scheme 1. Chemical Mechanisms for Phosphodiester Bond Hydrolysis Catalyzed by RNase H[a]

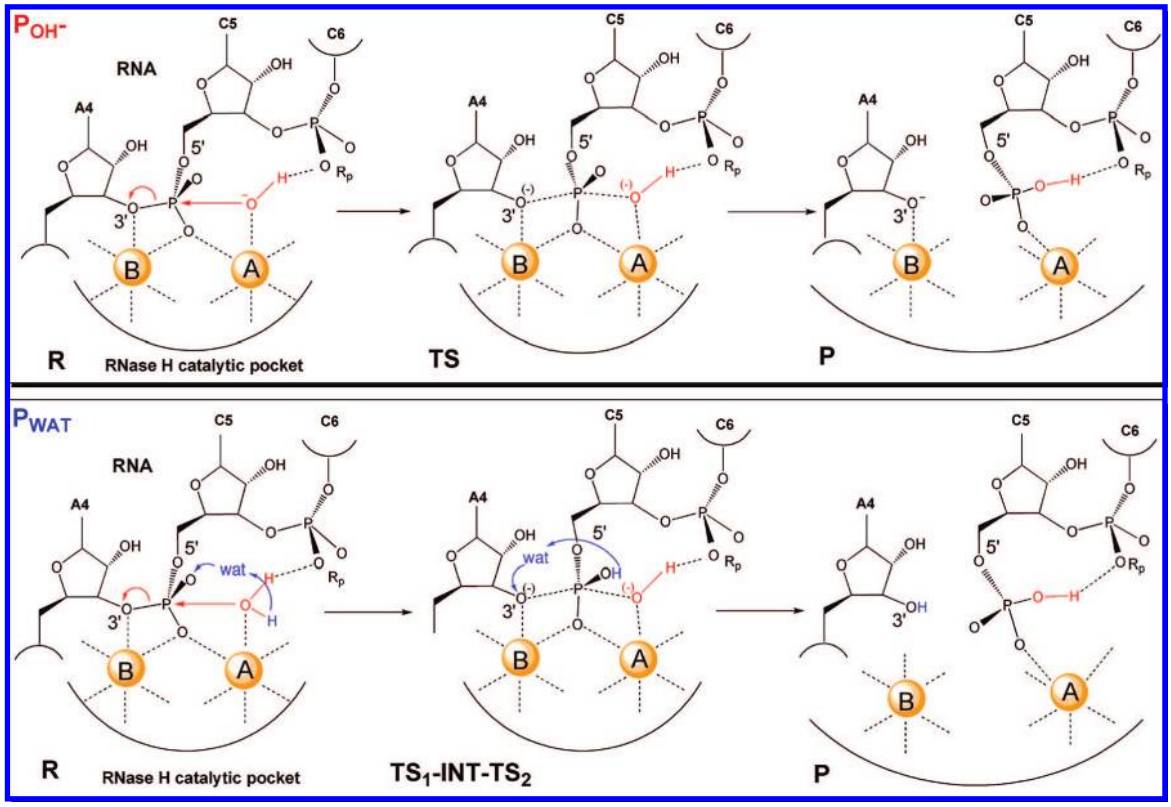

[a] Two nucleophilic agents are considered: water (WAT pathway, bottom) and hydroxide ion (OH^- pathway, top) (see also Figures 1 and 2). An in-line S_N2-like nucleophilic attack on the scissile phosphorus atom by the nucleophilic group is followed by the inversion of the phosphate stereo configuration and formation of the 5′-phosphate and 3′-hydroxy function of the RNA strand.

a very low rmsd with respect to the X-ray structure. From the equilibrated trajectory, a configuration featuring a nucleophilic hydroxyl ion (OH^-) has been built and run for ~1 ns, which was the time needed to relax the local H-bond network around the nucleophilic agent (the remaining structural determinants of the complex remained unchanged).

QM/MM MD Simulations. The reaction pathway is studied using QM/MM CP[25] dynamics:[20] the reactive region of the complex is treated at the quantum level (DFT-BLYP)[26,27] and includes namely the Mg^{2+} coordination sphere (DDED motif: D71, E109, D132, D192), part of the RNA A4, C5, C6 nucleotides, and solvation water molecules (Figure 2). Two starting structures derived from preparatory MD simulations are considered, in which the nucleophilic species is either a water molecule (WAT) or one nucleophilic hydroxide ion (OH^-). The remaining part of the complex is treated using classical force field.[21] The valence electrons are described by a plane wave basis set up to a cutoff of 70 Ry. A 20 × 20 × 18 $Å^3$ cell includes the QM part of the system. The interactions between valence electrons and ionic cores are described with norm-conserving Martins-Troullier pseudopotentials.[28] QM/MM CP dynamics are carried out with a time step of 0.12 fs (for a total run time of ~200 ps) and a fictitious electron mass of 500 au; constant temperature simulations are achieved by coupling the system with a Nosé-Hoover[29,30] thermostat at 500 cm^{-1} frequency. The interactions between the MM and QM regions are coupled in a Hamiltonian scheme as in ref 20. Notably, a rigorous Hamiltonian treatment of the electrostatic interaction between QM and MM regions is used as in ref 31. The approach has been shown to accurately describe a variety of enzymatic systems,[32,33] in particular metallo-enzymes and DNA complexes.[34–38] CP calculations have also been used to correctly predict relative pK_a values.[39,40]

QM/MM protocol includes an initial equilibration of the configuration produced by MD simulations, followed by a short run where only the MM part is free to move, while the QM part is kept frozen. Then, the whole system is allowed to move and heat up to 300 K (~2 ps); after that, trajectories are collected for analysis. Configurations from the equilibrated QM/MM simulations are used for free energy calculations. The phosphate transfer reaction is described with a reaction coordinate (RC) defined as the difference between the length of the forming bond (O_{nucl}−P) and that of the

(25) Car, R.; Parrinello, M. *Phys. Rev. Lett.* **1985**, *55* (22), 2471–2474.
(26) Becke, A. D. *Phys. Rev. A* **1988**, *38* (6), 3098–3100.
(27) Lee, C. T.; Yang, W. T.; Parr, R. G. *Phys. Rev. B* **1988**, *37* (2), 785–789.
(28) Troullier, N.; Martins, J. L. *Phys. Rev. B* **1991**, *43* (11), 8861–8869.
(29) Nosé, S. *J. Chem. Phys.* **1984**, *81* (1), 511–519.
(30) Hoover, W. G. *Phys. Rev. A* **1985**, *31* (3), 1695–1697.
(31) Laio, A.; VandeVondele, J.; Rothlisberger, U. *J. Phys. Chem. B* **2002**, *106* (29), 7300–7307.
(32) Carloni, P.; Rothlisberger, U.; Parrinello, M. *Acc. Chem. Res.* **2002**, *35* (6), 455–464.
(33) Dal Peraro, M.; Ruggerone, P.; Raugei, S.; Gervasio, F. L.; Carloni, P. *Curr. Opin. Struct. Biol.* **2007**, *17* (2), 149–156.
(34) De Vivo, M.; Ensing, B.; Dal Peraro, M.; Gomez, G. A.; Christianson, D. W.; Klein, M. L. *J. Am. Chem. Soc.* **2007**, *129* (2), 387–394.
(35) De Vivo, M.; Ensing, B.; Klein, M. L. *J. Am. Chem. Soc.* **2005**, *127* (32), 11226–11227.
(36) Dal Peraro, M.; Vila, A. J.; Carloni, P.; Klein, M. L. *J. Am. Chem. Soc.* **2007**, *129* (10), 2808–2816.
(37) Dal Peraro, M.; Llarrull, L. I.; Rothlisberger, U.; Vila, A. J.; Carloni, P. *J. Am. Chem. Soc.* **2004**, *126* (39), 12661–12668.
(38) Magistrato, A.; Ruggerone, P.; Spiegel, K.; Carloni, P.; Reedijk, J. *J. Phys. Chem. B* **2006**, *110* (8), 3604–3613.
(39) Davies, J. E.; Doltsinis, N. L.; Kirby, A. J.; Roussev, C. D.; Sprik, M. *J. Am. Chem. Soc.* **2002**, *124* (23), 6594–6599.
(40) Ivanov, I.; Chen, B.; Raugei, S.; Klein, M. L. *J. Phys. Chem. B* **2006**, *110* (12), 6365–6371.

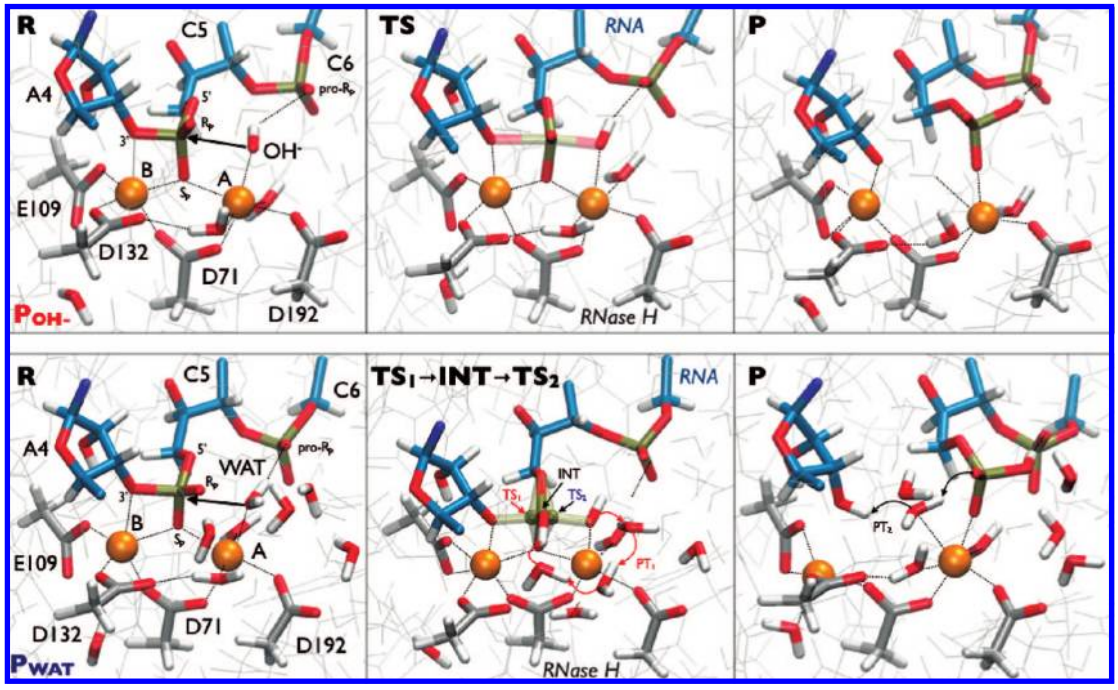

Figure 2. Structural evolution of the reaction. Selected snapshots taken for the QM/MM dynamics of the two investigated pathways for RNase H catalysis (only QM atoms are shown explicitly, the rest of the system is shown in thinner lines). (Top) OH^- pathway: the nucleophilic group is one hydroxide ion, **R**. The phosphorane-like **TS** is shown in the middle. Then, inversion of the phosphate stereo configuration and formation of the 5′-phosphate and 3′-hydroxy function of the RNA strand are shown in **P**. (Bottom) WAT pathway: the nucleophilic group is a water molecule, **R**. The nucleophilic attack leads to $\mathbf{TS_1}$, where a proton shuttle ($\mathbf{PT_1}$) involves 3 water molecules that bridge the scissile phosphate and WAT (red labels). The protonation of the scissile phosphate stabilizes the phosphorane group, causing the formation of the meta-stable intermediate **INT** (black label). Then, $\mathbf{TS_2}$ (blue label) leads to the final product **P**, in which the cleavage of the RNA strand is definitely completed, and the protonation of the 3′-hydroxy function of the RNA strand takes place ($\mathbf{PT_2}$).

breaking bond (P−O3′). This RC is well suited for S_N2-like reactions.[41,42] "Blue-moon" ensemble simulations are carried out adiabatically constraining the RC, while leaving all other degrees of freedom free to evolve. The free energy surface (FES) of the reaction is obtained by thermodynamic integration.[43] The pathway from reactants to products is divided in 14 steps, with a resolution of 0.2 Å that has been showed to lead to a reasonable compromise between accuracy and CPU-time consumption (additional steps with 0.1 Å resolution are considered in the vicinity of the intermediate states).[17,34,36] Each step is simulated for at least 5 ps, or until the force on the constraint is equilibrated (i.e., the running averages over 1 ps windows varies less than 5%). The MD-averaged force acting on the 1-D RC is plotted versus the length of the RC. The free energy profile is then obtained by integration of the force profile, leading to the description of the FES. The error associated to the critical points of FES is calculated by propagating the error on forces at every step, using the propagation of error formula for linear functions. The free energy values should be considered approximate due to the still limited sampling accessible to first principles DFT calculations, the choice of a 1-D RC, and the limitations of current GGA XC functionals. The catalytic pathways are then characterized in terms of the variation of critical bond lengths averaged over the equilibrated trajectory of each simulation step.

Results and Discussion

The X-ray structure of *Bh* RNase H in complex with hybrid RNA•DNA substrate shows that two Mg^{2+} ions are located in the active site where the cleavage of phosphodiester bond is catalyzed.[6] As mentioned above, MD is used to equilibrate the complex of the reconstructed wild type conformation starting from the D192N mutant crystallographic model.[24] RNase H is highly stable in the multi-nanosecond time scale (∼25 ns, 1.8(2) Å rmsd for the protein heavy atoms), whereas RNA•DNA substrate, although more flexible in solution (3.2(4) Å rmsd for heavy atoms), maintains unaltered interactions with the enzyme with respect to the crystal structure. Note, the coordination shells of the two metal ions are very well preserved and the position of the nucleophilic water, in the apical coordination of the A-site Mg^{2+} ion (MgA, Figure 1), is conserved throughout the entire simulation.[24]

Two different reagent states have been taken into account to study the enzymatic reaction: (i) one in which the nucleophilic species is a water molecule (WAT), and (ii) a second in which a hydroxide ion (OH^-) is the reactive nucleophile. For each pathway (P_{WAT}, and P_{OH^-}, respectively, Figure 2), constrained CP QM/MM simulations are performed to sample the reaction coordinate (RC) throughout the [−1.4, 1.4] Å spatial window needed to reach the product state. RC is defined as the difference between the length of breaking and forming bonds, RC = ($r1$ − $r2$), where $r1$ = P−O3′, and $r2$ = P−O_{WAT/OH^-}. The structural and energetic features of the reactions are summarized in Figures 2 and 3, whereas in Figure 4 structural comparisons with available X-ray data are shown.

OH^- Nucleophile Pathway (P_{OH^-}). The free energy surface (FES) shows two minima, reagents (**R**) and products (**P**), separated by a transition state (**TS**) maximum (Figures 2 and 3). In the **R** state, the system is stabilized by a well-structured H-bond network, which is centered on the two Mg^{2+} metal ions. The breaking bond is $r1 \approx 1.69$ Å, whereas the nascent bond

(41) Akola, J.; Jones, R. O. *J. Phys. Chem. B* **2003**, *107* (42), 11774–11783.
(42) Meijer, E. J.; Sprik, M. *J. Am. Chem. Soc.* **1998**, *120* (25), 6345–6355.
(43) Ciccotti, G.; Ferrario, M.; Hynes, J. T.; Kapral, R. *Chem. Phys.* **1989**, *129* (2), 241–251.

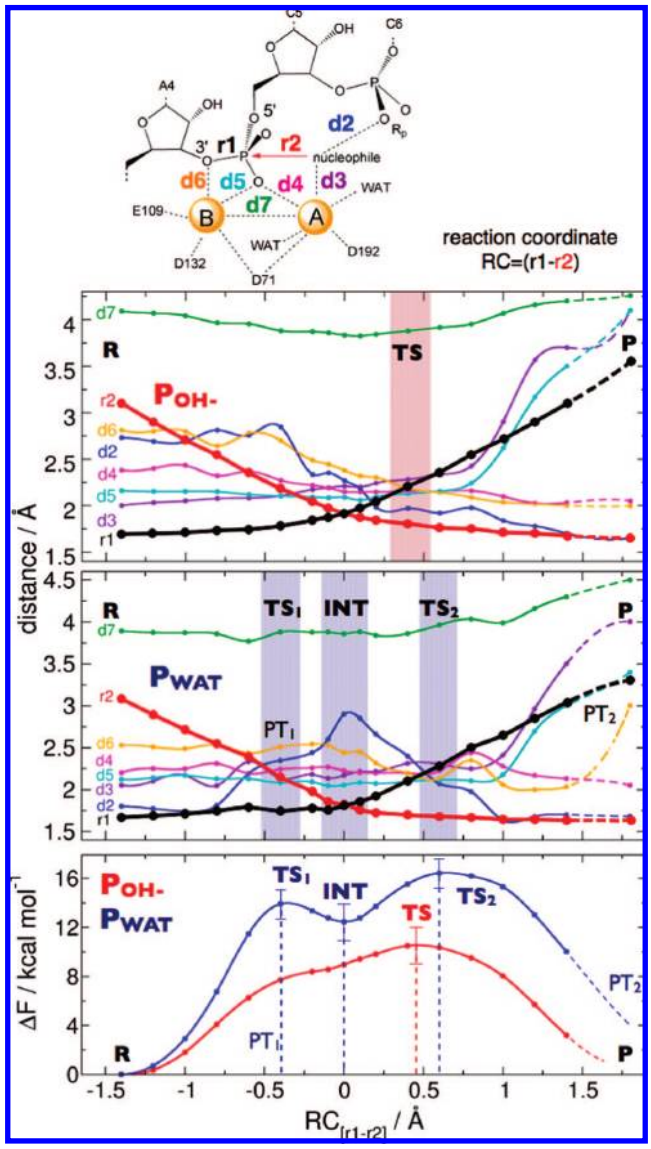

Figure 3. Structural and energetic properties of the reaction. Free energy profiles of the two investigated pathways for RNase H catalysis (bottom). Selected average bond distances of the pathway having one water (middle) or one hydroxide ion (top) as nucleophilic group. Bond distance labels as on the scheme at the very top. *r*1 and *r*2 are the breaking and forming P−O bond lengths describing the reaction, respectively, and are highlighted in bold lines.

is $r2 \approx 3.09$ Å. The internuclear distance between the two Mg^{2+} ions (*d7*) is 4.08 Å. From this point, RC is progressively decreased. At RC = 0 Å, the length of both *r*1 and *r*2 is 1.91 Å. *d7* decreases along the pathway, reaching the minimal value of 3.83 Å at RC = 0 Å. The variation of other significant distances (labeled as in Figure 3) indicates structural changes concomitant with the phosphoryl transfer; the distance between the B-site Mg^{2+} ion and the 3′ oxygen atom (*d6*) decreases, indicating a stabilization of the leaving 3′ oxygen. Simultaneously, the distance between the A-site Mg^{2+} ion and the bridging oxygen (*d4*) also decreases, as evidence that the OH^- group is approaching the scissile phosphorus. Also, the distance between the OH^- and the A-site Mg^{2+} ion (*d3*) progressively increases along the reaction pathway, further indicating that the OH^- group is approaching the scissile phosphorus. Finally, the distance between OH^- and the pro-R_p oxygen *(d2:* distance between the nucleophilic hydrogen and pro-R_p oxygen) decreases along the reaction pathway, indicating a strong H-bond that helps in maintaining the near-attack conformation of the OH^- group.

When RC = 0.4 Å (Figure 3), the transition state (TS) is reached. Here, *r*1 has a value of 2.20 Å, while *r*2 decreases to 1.80 Å, which indicates an associative mechanism for phosphoryl transfer. At this point, the two metal ions are 3.87 Å apart. At RC = 0.6 Å the system evolves downhill toward the product state (**P**) on the FES. At RC = 1.4 Å, the inversion of the phosphate stereo configuration and formation of the 5′-phosphate and 3′-hydroxy function of the RNA strand concludes the catalytic action. Upon removal of the RC constraint, the system falls into the product well, at a final value of RC ≈ 1.8 Å where *r*1 = 3.55 Å, and *r*2 = 1.64 Å. The product formation is accompanied by the shortening of distances *d4* and *d6* (∼2 Å), whereas *d3* and *d5* increase their values to ∼4.1 Å. The distance between the metal ions (*d7*) is slightly diverging at this stage, indicating a possible collapse of the active site architecture at the product state.

WAT Nucleophile Pathway (P_{WAT}). The nucleophilic agent considered in this pathway is a water molecule (WAT). The QM system includes also 12 solvation waters, previously treated at the MM level in the P_{OH^-}, that are forming an ordered H-bond network in the catalytic site. In this case, the FES shows three distinct minima: reagents (**R**), intermediate (**INT**), and products (**P**), separated by two transition states ($\mathbf{TS_1}$ and $\mathbf{TS_2}$). As in P_{OH^-}, in the **R** state, the system is stable and centered on the two Mg^{2+} ions. The bond in breaking *r*1 is 1.68 Å, whereas the bond in forming is ∼3.08 Å (Figures 2 and 3). The internuclear distance *d7* between the two ions is 3.90 Å. Interestingly, WAT allows a shorter internuclear distance between the two metal ions, in comparison to that showed in **R** of P_{OH^-} (4.08 Å).

At RC = −0.4 Å (Figure 3), the $\mathbf{TS_1}$ configuration is reached in which the average force on RC constraint is zero. The length of *r*1 is 1.75 Å, just slightly longer than that in the **R** state. However, *r*2 is now 2.15 Å, which indicates a bond is forming. Importantly, WAT loses one of its protons (PT_1), which is transferred to a nearby water molecule and not to the pro-R_p oxygen of RNA C6. Thus, the role of the pro-R_p oxygen is to maintain the right orientation of the nucleophile during the attack, while it does not act as a general base. The spontaneous proton transfer on a water molecule initiates a chain of fast (subpicosecond time scale) proton transfers that ultimately shuttles the proton to the R_p oxygen of the scissile phosphate. Three water molecules that bridge the scissile phosphate and WAT are involved in this proton shuttle. In principle, diverse paths for this proton shuttle could be possible, if a different H-bond network was formed. Nevertheless, this would likely not affect the mechanism for nucleophilic attack on the phosphate, since the proton shuttle is a barrier-less event. The internuclear distance *d7* between the two metals is 3.87 Å, as for the P_{OH^-} pathway. The other significant distances conserve their initial values; only *d2* shows an increment to 2.34 Å, which corresponds to a weakening of the H-bond formed with the pro-R_p oxygen.

When RC ∈ [−0.1, 0.1] Å, a metastable pentavalent phosphorane intermediate **INT** is formed, while the scissile phosphate remains protonated. At RC = 0 Å, both *r*1 and *r*2 are 1.82 Å, indicating the formation of a phosphorane species. At this point, *d2* reaches the maximum value of 2.9 Å, while the two Mg^{2+} ions are 3.85 Å apart. Interestingly, during $\mathbf{R \rightarrow TS_1 \rightarrow INT}$, *d7* decreases as in the previous pathway indicating that the two

metal ions are coming closer in a concerted fashion. This facilitates the phosphorane formation through an electrostatic stabilization of both the nucleophilc oxygen and the leaving 3′ oxygen atoms, which are both directly coordinated in apical positions to the two metals (Figure 2).

At RC = 0.6 Å (Figure 3), a second transition state **TS_2** is formed. The bond *r*2 is definitely formed, showing a length of 1.68 Å, while *r*1 is ∼2.28 Å. This late **TS_2** leads to the final product (**P**), in which the cleavage of the RNA strand is completed. Along **INT→TS_2→P**, the two ions are gradually falling apart, as shown by the constant increase of *d7*, passing from 3.85 Å in **INT** to 3.96 Å in **TS_2** and finally to 4.5 Å in **P** (Figure 3). The final formation of the 5′-phosphate leads to the decreasing of *d2* during the release of the product. Then, upon removal of the constraint, the system falls toward the final product. At this point we observe the protonation of the leaving 3′-hydroxy function, by the protonated 5′-phosphate: the proton on the scissile phosphate is transferred onto the leaving 3′ oxygen via a water wire mechanism, inducing the definitive release of the leaving group, which loses its coordination to the B-site Mg^{2+}, as indicated by the increase of *d6* (∼3 Å in **P**). Further indications of the formation of the final product are also the changes of distances *d3* and *d5* (∼4 Å and ∼3.4 Å in **P,** respectively), which increase along the reaction pathway.

Energetics of the Enzymatic Reactions. The FES of each of the investigated pathways (i.e., P_{WAT} and P_{OH^-}) is computed by thermodynamic integration as described in the method section; the resulting activation barriers are plotted in Figure 3. As expected, the lowest free energy barrier is obtained when the nucleophilic agent is a hydroxide (OH^-), where a one-step mechanism is observed (**R→TS→P**) with a $\Delta F = 10.5 \pm 1.1$ kcal mol^{-1} (Figure 3). A quasi-flat region of the FES is obtained in the interval RC ∈ [−0.1, 0.1] Å, in which we cannot rule out the presence of a meta-stable intermediate. However, when WAT is the attacking nucleophile as in P_{WAT}, a competitive free energy barrier is obtained (Figure 3) that clearly shows such a meta-stable intermediate. In fact, a stepwise profile **R→TS_1→INT→TS_2→P**, **INT** connects two distinct transition states, **TS_1** and **TS_2**. The rate-limiting step is **TS_2**, with a $\Delta F = 16.0 \pm 1.4$ kcal mol^{-1} higher than the reagent state **R**. **TS_1** has $\Delta F = 14.2 \pm 1.0$ kcal mol^{-1}, whereas **INT** is only ∼2 kcal mol^{-1} lower than **TS_1** ($\Delta F = 12.0 \pm 1.2$ kcal mol^{-1}). Thus, the FES of P_{WAT} indicates the existence of a pentavalent phosphorane intermediate such as that observed in β-phosphoglucomutase,[44–49] while the high energy of **INT** may be the reason why such an intermediate state has not been resolved yet by crystallography. Also, the pentavalent phosphorane intermediate has never been observed in previous computational studies performed on other phosphoryl transfer enzymes approached with similar techniques and level of theory, namely soluble epoxide hydrolase (sEH),[34,35] HIV-1 integrase,[50] and cyclin-dependent kinase 2 (CDK2).[51]

Interestingly, the relative stability of **INT** along P_{WAT} seems to be caused by the presence of a proton on the scissile phosphate in the transition region (**TS_1→INT→TS_2**) during catalysis. Indeed, the protonation of the scissile phosphate seems to stabilize the phosphorane formation, causing a lowering of its energy and the formation of the meta-stable intermediate **INT**. Conversely, this does not occur along P_{OH^-} where the scissile phosphate is always deprotonated.

It is important to notice that P_{WAT} implicitly includes the free energy needed for the dissociation of WAT observed at the point **TS_1**. The spontaneous WAT deprotonation indicates a low-energy barrier process. To compare the FES of the two pathways, P_{WAT} and P_{OH^-}, to a first approximation, one can account for the dehydration energy needed for the formation of the nucleophilic hydroxide group at the reagents state. We estimated the barrier of this event to be about 3 kcal mol^{-1}, using a constrained CP QM/MM calculation performed at **TS_1** (RC = −0.4 Å). Taking this into account, the two pathways might show a rate-limiting step with almost comparable energy (**TS** in P_{OH^-} could be as high as 13.5 kcal mol^{-1} vs 16 kcal mol^{-1} for **TS_2** in P_{WAT}). Hence, within the uncertainty related to the calculated free energy in our scheme, we cannot safely discard either pathway based on the energy profiles. Also, experimental data do not unambiguously prove the preference of one nucleophilic group versus the other: the optimum pH for RNase H activity is reported to be about 8, whereas the optimal Mg^{2+} concentration is ∼8 mM.[52,53] However, it is not clear how to relate these data to the protonation state of the nucleophilic group, which is likely more affected by local conditions in the catalytic site, namely by the presence of the Mg^{2+} ion, which can reduce the pK_a of the first Mg^{2+} solvation shell by several units, through its electrostatic and chelating effects.[54] Nevertheless, further studies would be needed and are in progress to investigate the pK_a of the nucleophile and surrounding groups during catalysis and its dependency on the local metal concentration.

Furthermore, the free energy values can be compared with kinetics data currently available for RNase H enzyme, although from another organism. Shaw-Reid et al. [5] measured the kinetic parameters of 4 substrate analogs for HIV-1 RNase H activity. The experimental k_{cat} values range from 1.01 to 0.11 min^{-1}, which correspond to a free energy range from ∼19.8 to ∼21.2 kcal mol^{-1}. It is reasonable to assume that these data provide an upper limit of the native catalytic rate in *Bh* RNase H, since a faster reaction (i.e., a higher k_{cat}) would be expected for the real substrate. However, it is not trivial to estimate the accuracy of the computed free energy barriers with respect to the value of the native catalytic rate, for which we have only an upper limit. The calculated FES might suffer by an underestimation that is intrinsic in our method within the DFT-BLYP level of theory.[55] On the other hand, the choice of a simple 1-D RC might cause an overestimation of the free energy barrier. Nonetheless, the computed barriers remain qualitatively consistent with the available kinetic data for substrate analogs for HIV-1 RNase H activity.

Finally, a comparison of the enzymatic barriers with that of the phosphoryl transfer reaction in water is useful in quantifying

(44) Allen, K. N.; Dunaway-Mariano, D. *Science* **2003**, *301*, 1184d.
(45) Allen, K. N.; Dunaway-Mariano, D. *Trends Biochem. Sci.* **2004**, *29* (9), 495–503.
(46) Blackburn, G. M.; Williams, N. H.; Gamblin, S. J.; Smerdon, S. J. *Science* **2003**, *301*, 1184c.
(47) Holmes, R. R. *Acc. Chem. Res.* **2004**, *37* (10), 746–753.
(48) Lahiri, S. D.; Zhang, G. F.; Dai, J. Y.; Dunaway-Mariano, D.; Allen, K. N. *Biochemistry* **2004**, *43* (10), 2812–2820.
(49) Tremblay, L. W.; Zhang, G. F.; Dai, J. Y.; Dunaway-Mariano, D.; Allen, K. N. *J. Am. Chem. Soc.* **2005**, *127* (15), 5298–5299.
(50) Cavalli, A.; De Vivo, M.; Recanatini, M. *Chem. Commun.* **2003**, (11), 1308–1309.
(51) De Vivo, M.; Cavalli, A.; Carloni, P.; Recanatini, M. *Chemistry* **2007**, *13* (30), 8437–8444.
(52) Lee, Y. I.; Hong, Y. B.; Kim, Y.; Rho, H. M.; Jung, G. *Biochem. Biophys. Res. Commun.* **1997**, *233* (2), 401–407.
(53) Wei, X.; Peterson, D. L. *J. Biol. Chem.* **1996**, *271* (51), 32617–32622.
(54) Lightstone, F. C.; Schwegler, E.; Hood, R. Q.; Gygi, F.; Galli, G. *Chem. Phys. Lett.* **2001**, *343* (5−6), 549–555.
(55) Zheng, J.; Zhao, Y.; Truhlar, D. G. *J. Chem. Theory Comput.* **2007**, *3*, 569–582.

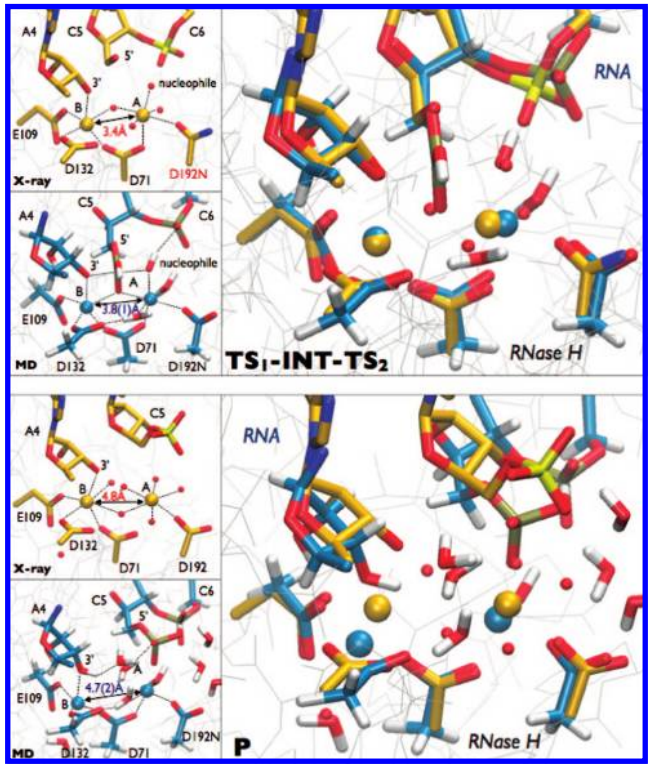

Figure 4. Structural comparison of intermediate and product states with available crystallographic data. Superimposition of representative structures of the transition state region (TS_1, INT, TS_2) (top) and the product state (bottom) from the pathway having a water as nucleophile (P_{WAT}) with the intermediate-like (top) and product-like (bottom) crystallographic structures, respectively, as reported in ref 8.

the catalytic power of the RNase H enzymatic mechanism. For our case, the study of Akola and Jones[41] is the most relevant because it concerns the hydrolysis of the Mg^{2+}-complexed methyl thiophosphate in water, studied by means of CPMD calculations. The barriers found for different mechanisms (dissociative and associative) are ~35−40 kcal mol^{-1}. Thus, this result further shows the efficiency of the enzymatic mechanisms proposed herein.

Role of Mg^{2+} Metal Ions. The two metals act simultaneously in order to promote and facilitate an efficient catalysis as in P_{OH^-} and P_{WAT}. In fact, the distance between the ions decreases along the reaction pathway, from the reactants to TS, as shown in Figure 3. After **TS** or **INT** states, the two metals start to relax to their original positions, until the release of the product leads to an even longer distance (4.7 Å, Figure 4) which likely precedes a collapse of the complex, with eventually complete solvation and release of the metal ions from the catalytic pocket.

Nowotny and Yang,[1,6,8] based on crystallographic evidence, suggested previously this cooperative behavior of the two metal ions. Importantly, our calculations confirm that the two metal ions have a different role, while behaving in a cooperative fashion. In particular, the A-site Mg^{2+} conserves the ideal octahedral coordination along the entire pathway, thus stabilizing the nucleophile near-attack conformation. Interestingly, the coordination of the B-site Mg^{2+} is slightly irregular: its starting coordination includes five ligands, which would induce a less-stable coordination shell. However, the metal coordination of D132 changes from monodentate to bidentate a few times (i.e., 5 or a 6 ligands-shell coordination) along the simulations. Thus, the B-site Mg^{2+} plays a dual role: stabilizing the leaving group after phosphodiester bond cleavage and likely destabilizing the

Scheme 2. Metal Content and Nature of the Reaction[a]

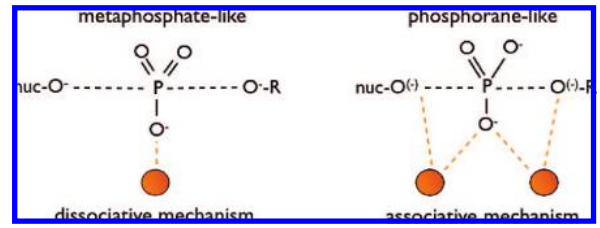

[a] Different mechanisms for phosphoryl-transfer (associative *vs.* dissociative) might be induced by the metal(s) position and stochiometry at the TS. The metaphosphate-like TS, typical for a dissociative mechanism, is stabilized by its apical coordination to the only Mg^{2+} ion present in the catalytic site as reported in refs 33, 34. Conversely, in the RNase H catalysis, the position of the two Mg^{2+} cations stabilizes the attacking and leaving groups, while the metaphosphate group is accommodated between the two metals, forming a phosphorane-like TS geometry.

substrate-enzyme complex, as suggested by Nowotny and Yang.[1,6,8] Finally, we also observed the hydration of the A-site Mg^{2+} coordination shell upon reaching the product state, where water molecules saturate the metal octahedral coordination, according to the crystallographic hypotheses.

Overall, the present computations offer a striking confirmation of the mechanistic hypotheses based on the crystallographic findings of Nowotny and Yang,[1,6–8] as shown by the superimpositions of structures reported in Figure 4. Both the **TS** in P_{OH^-} and **TS_1→INT→TS_2** multiple state in P_{WAT} are remarkably similar to the X-ray "intermediate" state[8] (rmsd ≈ 0.7 Å for the metal site) proposed by the crystallographers. Only one subtle discrepancy, namely, the internuclear distance of the two Mg^{2+} ions, is observed. In fact, calculations provide a 3.8(1) Å separation between the two ions, whereas in the crystals the distance is ~3.4 Å. This is likely due to the fact that the X-ray "intermediate" crystal structure[8] lacks the scissile phosphate group so as to impair the enzymatic activity and allow the resolution of the complex. This gap, partially filled by a water molecule, likely allows the two metal ions to stay closer than in the true reactive/intermediate state. First principles calculations implicitly account for steric and electronic contributions of the phosphodiester group between the two metal ions along the reaction pathway and support a slightly longer internuclear distance at the intermediate state.

The agreement between the product state proposed based on crystallographic data and the computed one, as shown by the superimpositions reported in Figure 4, is remarkable. An increasing metal−metal distance is observed with their partial solvation and the release of RNA hydrolyzed strand outside the catalytic cleft. Overall, the crystallographic structure seems slightly more advanced toward the final product release.

An interesting point regarding the role of the Mg^{2+} ion(s) in catalyzing phosphoryl-transfer reactions can be observed by comparing these results with a recent study of ours,[34] which uses an identical computational approach for investigating the enzymatic activity of the soluble epoxide hydrolase (sEH). The catalytic site of sEH includes only one Mg^{2+} cation, instead of two ions as in the case of RNase H. Although the type of catalyzed reaction (i.e., phosphoryl transfer) is the same in both enzymes, the observed TS geometry is different: the RNase H catalysis shows an associative phosphorane-like TS, whereas the sEH catalysis shows a rather metaphosphate-like TS/intermediate. We suggest that this difference is induced by the position of the metal(s) in the TS. In fact, during the sEH catalysis, the metaphosphate group that is transferred is stabilized

by its apical coordination to the only Mg^{2+} ion present in the catalytic site (Scheme 2). On the other hand, in the RNase H catalysis, the two Mg^{2+} cations stabilize the attacking and leaving groups, while the metaphosphate group is accommodated between the two metals, forming a phosphorane-like TS geometry (Scheme 2). Thus, different mechanisms for enzymatic phosphoryl transfer (associative versus dissociative) might be generally induced according to the metal(s) stochiometry and geometry. This hypothesis, however, is still speculative at this point and needs more accurate and extended mechanistic investigations to be supported.

Conclusion

We present mechanistic details and the free energy profile of the enzymatic activity of RNase H, which hydrolyzes the P−O3′ bond of the RNA strand in RNA•DNA hybrids. A key point is that the two Mg^{2+} cations, which are required for activity, are playing a concerted role in the catalysis.

Two pathways, which differ on the nature of the nucleophile, have been studied: (i) P_{OH^-} where a hydroxide ion (OH^-) is the nucleophilic agent, and (ii) P_{WAT} where it is a water molecule (WAT). As expected, due to the high basicity of the OH^- group, P_{OH^-} shows the lowest free energy barrier ($\sim$10.5 kcal mol^{-1}). Nevertheless, P_{WAT} shows a competitive mechanism (free energy barrier $\approx$ 16 kcal mol^{-1}) if dehydration energy is also taken into account and could provide a favorable mechanism if the pK_a condition at the active site would not allow an early nucleophilic deprotonation, which is a necessary chemical step in order to have a reactive species. Crucially for the latter mechanism, the formation of the nucleophilic OH^- is caused by the migration of one proton of WAT to the R_p oxygen of the scissile phosphate. This proton is shuttled by three solvation water molecules that bridge the nucleophile and the phosphate at the transition state. Later, the proton is transferred onto the 3′-hydroxy group, during the final product release (Figures 2, 4). This final proton transfer is water-mediated, too. Thus, in agreement with recent studies,[34,35] water molecules solvating the metal center facilitate the migration of protons involved in the phosphoryl transfer reaction.

Both P_{OH^-} and P_{WAT} show an in-line S_N2-like nucleophilic attack on the scissile phosphorus, in agreement with stereochemical studies.[15] This leads to an associative mechanism with phosphorane-like transition states, in excellent agreement with crystal structures of TS analogues.[56,57] Importantly, P_{WAT} includes a meta-stable pentavalent phosphorane intermediate; such intermediate, however, could be present along P_{OH^-}, as well, and represents a unique characteristic of the free energy profile of the RNase H catalysis. In fact, it was never observed in previous computational studies of phosphoryl transfers catalyzed by other enzymes (i.e., soluble epoxide hydrolase (sEH),[34,35] HIV-1 integrase,[50] and cyclin-dependent kinase 2 (CDK2)[51]), whereas it resembles the debated crystal structure that shows a pentavalent phosphorane in β-phosphoglucomutase.[58] Although a real intermediate has never been solved for RNase H, likely because of the intrinsic high free energy that characterizes it, our structural findings are also consistent with the TS analogues resolved for RNase H[8] (Figure 4) and could be used for designing TS-analogue inhibitors.

The debated role of the pro-R_p oxygen during catalysis is also clarified: it does not seem to act as a general base in deprotonating the nucleophilic water, but it does support the reaction by maintaining the near-attack orientation of the nucleophilic group (either a water or hydroxide), in agreement with the recent hypothesis of Nowotny and Yang.[1,8] Also, the H-bond between the pro-R_p oxygen and nucleophilic water most likely decreases the pK_a of the nucleophile, inducing an easier deprotonation and enhancing the catalytic efficiency.

Our findings show that the two Mg^{2+} ions act in a cooperative fashion, representing indeed an essential aspect of the reaction mechanism. In fact, they act simultaneously to promote and facilitate both nucleophile formation and leaving group stabilization. As a main result, both P_{OH^-} and P_{WAT} show a phosphorane-like transition state in which the associative character of the TS is supported by the two ions, which get closer to each other in the TS geometry. Based on this evidence, we suggest that different mechanisms (associative vs dissociative) for phosphoryl-transfers could be induced according to the metal(s) geometry and stochiometry during catalysis (Scheme 2).

In conclusion, our computational results complete the mechanistic hypotheses based on the crystallographic findings obtained by Nowotny and Yang.[1,8] Key aspects of the enzymatic activity of RNase H, such as the mechanism and energetics of nucleophile formation and the role of the metals during catalysis, have been explicitly thermodynamically characterized via first principles molecular dynamics. Due to the conservation of this bimetal motif in other classes of structurally similar enzymes that incorporate in their sequence the conserved DDE motif, the results presented herein might be valid for the enzymes belonging to the NT superfamily. The knowledge of transition state geometries and water dynamics is also of practical interest, because they might eventually be exploited for the design of specific transition state analogue inhibitors targeting RNase H and/or homologues enzymes.[59]

Acknowledgment. We thank the NIH for financial support and the Pittsburgh Supercomputer Center (PSC) for computing time on the Cray XT3 machine. We also thank Bradley P. Feuston for stimulating discussions.

Supporting Information Available: Classical MD set up, rmsd's, and average distances at the catalytic site. This material is available free of charge via the Internet at http://pubs.acs.org.

JA8005786

(56) Schlichting, I.; Reinstein, J. *Biochemistry* **1997**, *36* (31), 9290–9296.
(57) Schlichting, I.; Reinstein, J. *Nat. Struct. Biol.* **1999**, *6* (8), 721–723.
(58) Lahiri, S. D.; Zhang, G. F.; Dunaway-Mariano, D.; Allen, K. N. *Science* **2003**, *299* (5615), 2067–2071.
(59) Cavalli, A.; Carloni, P.; Recanatini, M. *Chem. Rev.* **2006**, *106* (9), 3497–3519.